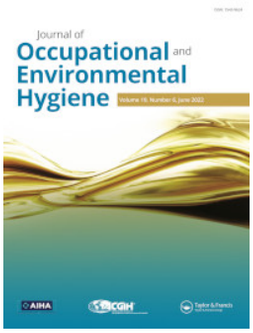

Journal of Occupational and Environmental Hygiene

ISSN: (Print) (Online) Journal homepage: https://www.tandfonline.com/loi/uoeh20

Asbestos fiber length and width comparison between manual and semi-automated measurements

Taekhee Lee, Teresa Barone, Elaine Rubinstein & Steven Mischler

To cite this article: Taekhee Lee, Teresa Barone, Elaine Rubinstein & Steven Mischler (2022) Asbestos fiber length and width comparison between manual and semi-automated measurements, Journal of Occupational and Environmental Hygiene, 19:6, 370-380, DOI: 10.1080/15459624.2022.2063878

To link to this article: https://doi.org/10.1080/15459624.2022.2063878

Published online: 05 May 2022.

JOURNAL OF OCCUPATIONAL AND ENVIRONMENTAL HYGIENE
2022, VOL. 19, NO. 6, 370–380
https://doi.org/10.1080/15459624.2022.2063878

Asbestos fiber length and width comparison between manual and semi-automated measurements

Taekhee Lee[a], Teresa Barone[a], Elaine Rubinstein[b], and Steven Mischler[a]

[a]Health Hazards Prevention Branch, Pittsburgh Mining Research Division, National Institute for Occupational Safety and Health, Centers for Disease Control and Prevention, Pittsburgh, Pennsylvania, USA; [b]Human Systems Integration Branch, Pittsburgh Mining Research Division, National Institute for Occupational Safety and Health, Centers for Disease Control and Prevention, Pittsburgh, Pennsylvania, USA

ABSTRACT

The objective of the present study is to find a fast and accurate procedure to measure the length and width of asbestos fibers using images acquired by a scanning electron microscope (SEM), a phase-contrast microscope (PCM), and a polarized light microscope (PLM). The accuracy of the procedure was evaluated by comparing fiber length and width measurements to manual measurements. Four different types of images were used in the evaluation: (1) backscattered electron SEM images of fibrous tremolite, (2) secondary electron SEM images of fibrous grunerite, (3) PCM images of fibrous grunerite, and (4) PLM images of fibrous grunerite. Fiber length and width were measured with ImageJ (manual measurement) and Image-Pro software and were compared on an individual fiber basis and over the number-length and number-width distribution of each sample. The results of the comparison showed that the individual length and width measurements with ImageJ and Image-Pro software had a nearly 1:1 relationship except for the width measurement in PLM images (8% of the variance in ImageJ width measurements was not explained by Image-Pro width measurements). Similarly, the number-length distributions were not significantly different ($p > 0.05$) between ImageJ and Image-Pro, but the number-width distributions were significantly different ($p < 0.05$) for PLM and secondary electron SEM images. Although the image analysis procedure for measuring fiber length and width with Image-Pro is not a fully automated procedure and still requires some manual intervention, it can be a more efficient and equally accurate alternative to time-consuming manual fiber length and width measurements for well dispersed fibers with high aspect ratios.

KEYWORDS

Asbestos; image analysis; ImageJ; Image-Pro

Introduction

Asbestos consists of a particular group of fibrous minerals that are known carcinogens used in past commercial products, rather than a comprehensive set of fibrous minerals (Baumann et al. 2013). Specifically, regulated asbestos includes only 6 of 400 naturally occurring fibrous minerals that may be encountered in occupations such as road construction, mining, and tunneling (Skinner et al. 1988; Baumann et al. 2013). Considering the potential for occupational exposures, regulated asbestos, and unregulated fibrous minerals are currently being studied with the objective of understanding their adverse effects on health (Lee et al. 2020, 2021). These studies involve systematically testing fiber properties and controlling sample characteristics.

The characterization of asbestos requires information on fiber morphology and minerology (Skinner et al. 1988). This information can be obtained by transmission electron microscopy (TEM) through imaging and selected area diffraction (Baron 2016). However, TEM analysis is often cost-prohibitive due to instrument acquisition, maintenance, and training expenses. Lower cost methods, such as phase-contrast microscopy (PCM), lack mineral identification capabilities but suggest the presence of asbestos through the analysis of fiber length and width (Baron 2016). Fiber length is an important metric because long fibers can impair macrophage function and reduce lung clearance (Blake et al. 1997). Width is also influential because (together with length) it affects location of deposition in the respiratory system and the nature of associated respiratory diseases (i.e., mesothelioma, asbestosis, and lung cancer) (Lippmann 1988). When

CONTACT Taekhee Lee fwc8@cdc.gov Health Hazards Prevention Branch, Pittsburgh Mining Research Division, National Institute for Occupational Safety and Health, Centers for Disease Control and Prevention, 626 Cochrans Mill Road, Pittsburgh, PA 15236, USA

Table 1. Methods and materials used for the comparison of ImageJ and Image-Pro measurements of asbestos fibers.

Method	Image type	Asbestos type	Number analyzed for individual fiber comparison	Number analyzed for size distribution with ImageJ	Number analyzed for size distribution with Image-Pro
FESEM	Backscattered electron	Fibrous tremolite	207	–	–
FESEM	Secondary electron	Fibrous grunerite	112	503	525
PCM	–	Fibrous grunerite	–*	–*	–*
PLM	–	Fibrous grunerite	216	198	217

* Omitted because lack of consistent contrast of fibers with the background.

linking fiber characteristics to adverse health effects, information on both length and width is critical.

Fiber length and width measurements are primarily made through image analysis. Image analysis should be carried out on a sufficiently large number of fibers to obtain length and width information, which is a time-consuming and tedious process when done manually. Automated methods have reduced this burden, but most have been limited to measuring either fiber length or width due to the specificities of their applications outside of asbestos analysis. Specifically, fiber length applications have involved the automated analysis of fibers used in reinforced composites (Hartwich et al. 2009; Goris et al. 2018; Liu et al. 2020) and polymer fibers found in environmental samples (Primpke et al. 2019). On the other hand, the automated analysis of fiber width has been developed for the characterization of overlapping fibers in muscle tissue (e.g., Stevens et al. 2020) and electrospun materials (Zhang et al. 2014; Hotaling et al. 2015; Murphy et al. 2020; Götz et al. 2021).

A few automated methods have been developed for determining fiber length and width concurrently. One of these was developed for the characterization of asbestos fibers imaged by scanning electron microscopy (SEM) (Cossio et al. 2018). Another was developed for the analysis of textile fibers imaged by optical microscopy (Xu and Ting 1996). Both have the advantage of addressing a wide range of fibers including curved fibers, such as microscopic chrysotile asbestos. However, disadvantages include the lack of accessibility as commercially available or open-source software and the necessity of using specialized hardware, such as lanthanum hexaboride or a field emitter instead of a tungsten filament as the electron beam source in the SEM. These implementation challenges may preclude their use by individual laboratories.

The benefits of accessible and low-cost image analysis methods have been detailed in a retrospective publication on the 25-year success of National Institutes of Health (NIH) Image and ImageJ (Schneider et al. 2012). Following this perspective, an automated method for fiber length and width measurements would ideally take the form of an open-source plugin, as has been done for width only by Hotaling and colleagues (2015). However, to the authors' knowledge, a compatible plugin or other open-source software for concurrent measurements of projected fiber length and width has not been made available. Alternatively, commercially available software, such as Image-Pro (Media Cybernetics, Inc., Rockville, MD) may be employed. Image-Pro has been previously used for nano- and micro-fiber width measurements to characterize scaffolds for nerve regeneration (Wang et al. 2008). In addition, a customized module for Image-Pro was developed for automated glass-fiber-length measurements (Hartwich et al. 2009). Furthermore, it has been applied for the automated analysis of features in composite material and biological samples (Ma et al. 2008; Fritzsch et al. 2013; Fujimoto et al. 2016; Reedy et al. 2017). Although Image-Pro was applicable in these studies, its suitability for the automated analysis of asbestos is unknown because the nature of the sample and substrate affects the performance of an image analysis system.

In the current study, Image-Pro was evaluated for its accuracy in characterizing the projected length and width of asbestos fibers in images acquired by lower cost methods relative to TEM, including PCM, polarized light microscopy (PLM), and SEM. The evaluation was carried out using straight asbestos fibers of tremolite and grunerite. Straight fibers were used because five of the six types of regulated asbestos have acicular (needle-like) morphology (Skinner et al. 1988), and the samples provide a less ambiguous assessment of the software's capabilities. The current assessment was carried out to determine whether Image-Pro along with PCM, PLM, or SEM would provide an accessible method for characterization of asbestos and other fibrous minerals.

Materials and methods

Images for analysis

Four different types of images were utilized in the present study (Table 1): (1) backscattered electron

images of fibrous tremolite (Harper et al. 2015) acquired with a field emission SEM (FESEM, S-4800-2, Hitachi High Technologies America Inc., Schaumburgh, IL); (2) secondary electron images of fibrous grunerite, known as amosite, from the asbestos mines of South Africa (NIOSH 1979) obtained with the FESEM; (3) phase contrast microscope (PrimoStar, Zeiss, Oberkochen, Germany) images of fibrous grunerite; and (4) polarized light microscope (BX-50, Olympus, Center Valley, PA) images of fibrous grunerite. The secondary electron FESEM, PCM, and PLM images of fibrous grunerite were obtained through our previous study on separating fibrous grunerite by its length using the filtration and shaking method (Lee et al. 2021).

Samples for the SEM analysis were deposited on polycarbonate membrane (PC; 0.4-μm pore size, 25 mm, Sterlitech, Kent, WA) filters after sonication for 10 min. Samples for the PCM and PLM analysis were prepared using microscope glass slides, cover slips, and triacetin. The number of fibers in each sample was measured using a PCM, and the samples were diluted or concentrated to yield approximately 50 fibers/field for PCM (at 400× magnification), PLM (at 400× magnification), and SEM (at 2,000× magnification) analysis.

Fiber length and width measurement

The length and width of fibers were measured with the following two different methods: (1) the manual method with ImageJ software (Version 1.48v, NIH, Schneider et al. 2012) and (2) the semi-automated method with Image-Pro (Version 10.0.7, Media Cybernetics Inc., Rockville, MD). The following steps were conducted for the Image-Pro software analysis: (1) spatial calibration using a scale bar in each image; (2) maximization of contrast between background and fibers by changing the image histogram; (3) application of either a Sigma filter to soften an image by replacing each pixel with an average of neighboring pixels or a Gaussian filter to soften an image by eliminating high-frequency information; (4) group segmentation to identify and isolate fibers in the images; and (5) measurement of isolated fibers' length and width. For the comparison of the length and width of individual fibers, each fiber measured by the above process using Image-Pro was identified, and its length and width were measured with ImageJ software after setting the scale using a scale bar in each image.

Length and width measurements were made for each type of image as described below and in Table 1.

1. A total of 207 fibrous tremolite asbestos fibers in 10 different backscattered FESEM images were measured using both software types for the individual fiber length and width comparison.
2. A total of 112 fibrous grunerite asbestos fibers in nine different FESEM secondary electron images were measured using both software types for the individual fiber length and width comparison. To compare fiber length and width distributions between the software types, a total of 503 and 525 fibrous grunerite length and width measurements, respectively, in 36 different secondary electron FESEM images were determined by both ImageJ and Image-Pro software. The length and width distributions determined by ImageJ software were reported previously (Lee et al. 2021). The image analysis using ImageJ and Image-Pro software were conducted by different investigators.
3. A total of 216 grunerite fibers in five different PLM images were measured using both software types for the individual fiber length and width comparison. To compare fiber length and width distributions, a total of 198 and 217 grunerite fibers in seven different PLM images were measured by ImageJ and Image-Pro software, respectively. Different investigators conducted the image analysis using ImageJ and Image-Pro software.

The PCM images of fibrous grunerite were omitted from further evaluations because the fiber detection rate with Image-Pro software was relatively lower than the detection rate for SEM and PLM images. Linear regression analysis was used to assess the consistency of length and width measurements between the two software types. Because all of the distributions of length and width measurements were skewed, regression analyses were performed on log transformed data to better meet the assumptions of normality of residuals and constant variance of residuals. Measured length and width distributions produced by the two types of software were compared by the Kolmogorov-Smirnov test. Data analysis was performed using [SAS/STAT] software, Version 9.4 of SAS for Windows (SAS Institute Inc., Cary, NC). A significance level of 0.05 was used for all statistical tests.

Results and discussion

Backscattered electron FESEM images

Scatter plots of fibrous tremolite length and width measured with ImageJ and Image-Pro (n = 207) are shown in Figure 1. The results of the linear regression analyses are summarized within the plot area. The measured length of tremolite ranged from 0.9 to 80 µm, and the measured width of tremolite ranged from 0.2 to 7 µm with both software. The slopes of the regression lines for both length and width, 0.98 and 0.95, respectively, were close to 1, and the intercepts of both regression lines, 0.04 and 0.03, respectively, were close to 0. These results suggest a nearly one-to-one relationship because in a one-to-one relationship the lower and upper bonds of a 95% confidence interval for the population slope and intercept are expected to span 1 and 0, respectively. For fiber length the value of R^2, 0.99, was virtually equal to 1, indicating that ImageJ measurements could be predicted from Image-Pro measurements with negligible error. The value of R^2 for width, 0.94, was slightly lower, but still high, indicating that approximately 94% of the variation in ImageJ measurements could be explained by Image-Pro measurements. Detailed results of the linear regression analyses for length and width are shown in Table 2, including 95% confidence intervals for the population slope and intercept.

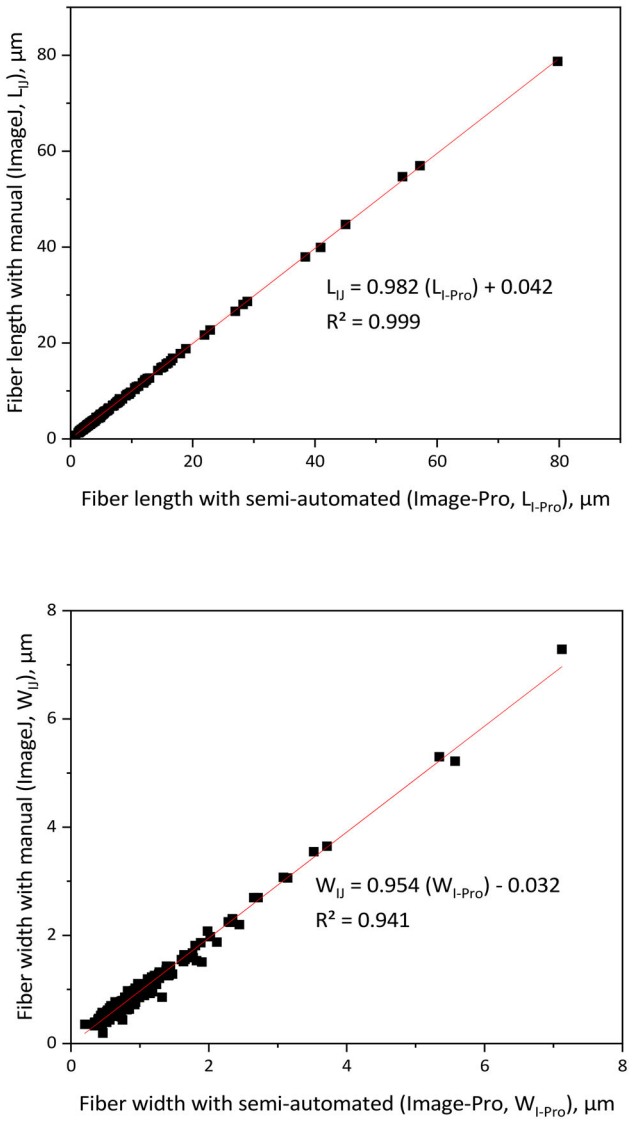

Figure 1. Scatter plots and linear regression analysis of tremolite asbestos length and width measured with ImageJ and Image-Pro (n = 207, backscattered FESEM images).

It should be noted that when a fiber was attached to or overlapped with other fiber(s), the Image-Pro software recognized the composite as one fiber and gave an incorrect measurement. Figure 2 shows two cases where a fiber was attached to or overlapped with other fiber(s) and displays three measurements of fiber width for each case: (1) ImageJ manual measurement, (2) Image-Pro semi-automated measurement when several fibers were attached or overlapped, and (3) Image-Pro manual measurement. Those fibers (#2) were identified individually and the lengths and/or widths were measured again with Image-Pro software and replaced with corrected one(s) (#3).

SEM secondary electron images

Scatter plots of amosite asbestos length and width measured with ImageJ and Image-Pro (n = 112) are shown in Figure 3. The results of the linear regression analyses are summarized within the plot area. The measured length of fibrous grunerite ranged from 0.8 to 22 µm and the measured width of fibrous grunerite

Table 2. Linear regression analysis results of individual fiber length and width between ImageJ and Image-Pro.

				95% confidence interval			
				Slope		intercept	
	Slope (p)	Intercept (p)	R^2	lower	upper	lower	upper
Tremolite length with backscattered SME image	0.982 (<0.0001)	0.042 (<0.0001)	0.999	0.978	0.987	0.034	0.050
Tremolite width with backscattered SME image	0.954 (<0.0001)	−0.032 (0.0007)	0.941	0.921	0.986	−0.050	−0.014
Fibrous grunerite length with secondary electron SEM image	1.004 (<0.0001)	−0.016 (<0.0001)	0.999	0.999	1.009	−0.023	−0.008
Fibrous grunerite width with secondary electron SEM image	0.981 (<0.0001)	0.005 (0.7147)	0.968	0.947	1.014	−0.021	0.030
Fibrous grunerite length with PLM image	1.019 (<0.0001)	−0.058 (<0.0001)	0.998	1.012	1.025	−0.073	−0.042
Fibrous grunerite width with PLM image	0.841 (<0.0001)	0.034 (<0.0001)	0.918	0.807	0.875	0.017	0.051

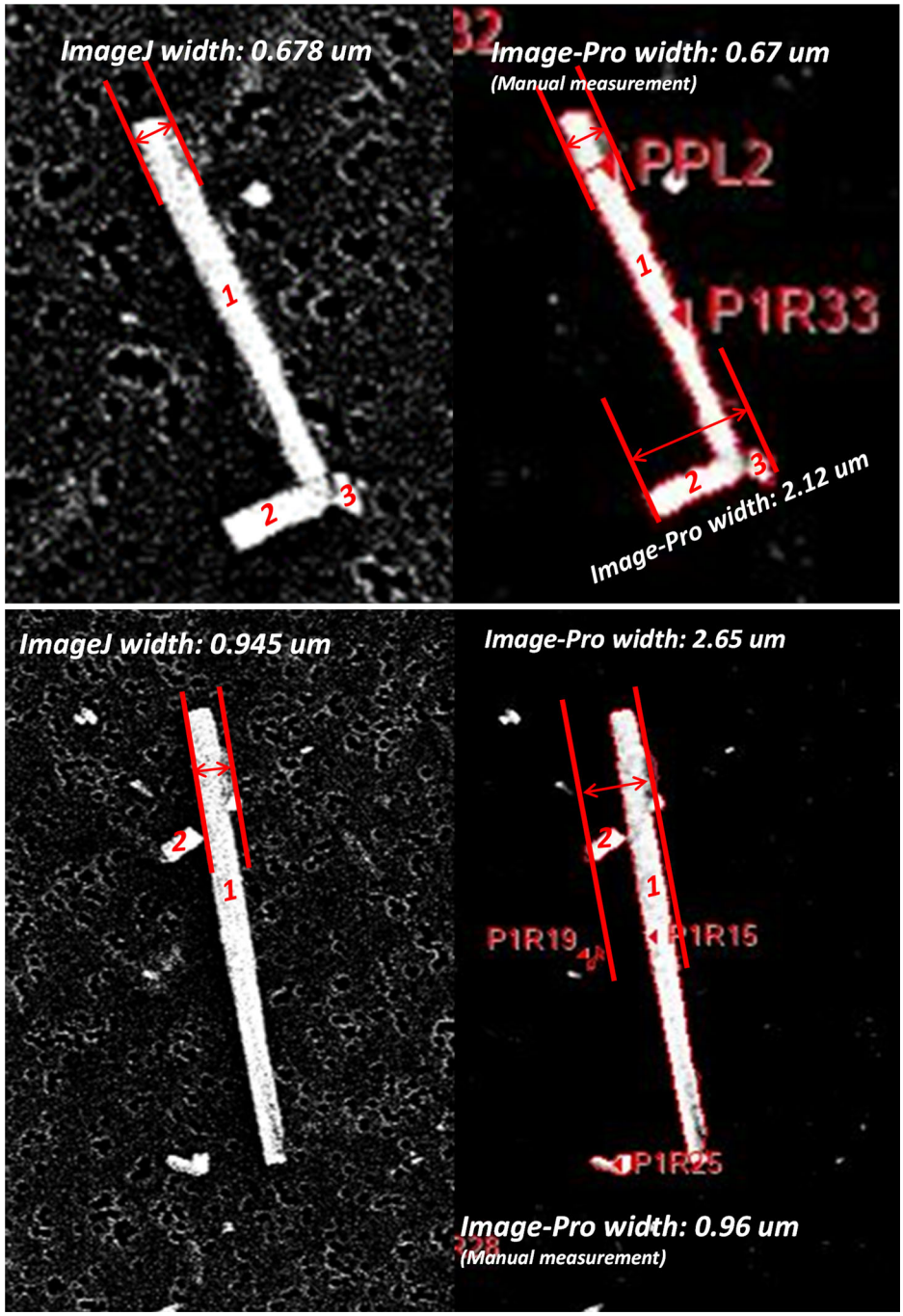

Figure 2. Examples of differences between ImageJ and Image-Pro software measurements of fiber widths when fiber(s) were attached to or overlapped with other fibers.

ranged from 0.2 to 1.3 µm with both software. Rounded to two decimal places, the slope of the regression line for length was 1.00 and the intercept was −0.02; for width, the values of the slope and intercept were 0.98 and 0.00, respectively. Thus, results for both length and width are consistent with a nearly one-to-one relationship. The coefficients of determination (R^2) in the regressions for length and width were also close to one, 0.99 and 0.97, respectively, indicating that virtually 100% of the variance in length and 97% of the variance in the width of ImageJ measurements are explained by Image-Pro measurements (Table 2). Normalized and cumulative fibrous grunerite length and width distributions in two different sets are shown in Figures 4 and 5, respectively. These figures display both measurements made with Image-Pro in 36 SEM secondary electron images (n = 525) and measurements made manually with ImageJ in 36 SEM images (n = 503). The manual measurements were reported previously (Lee et al. 2021). A Kolmogorov–Smirnov test

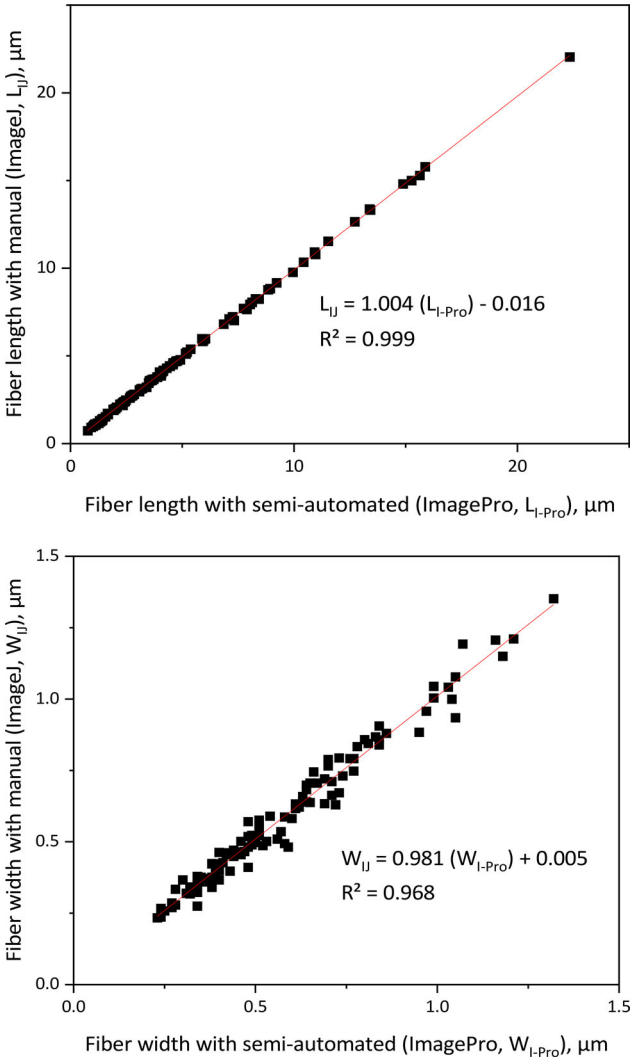

Figure 3. Scatter plot and linear regression analysis of amosite asbestos in length and width measured with ImageJ and Image-Pro (n = 112, secondary electron FESEM images).

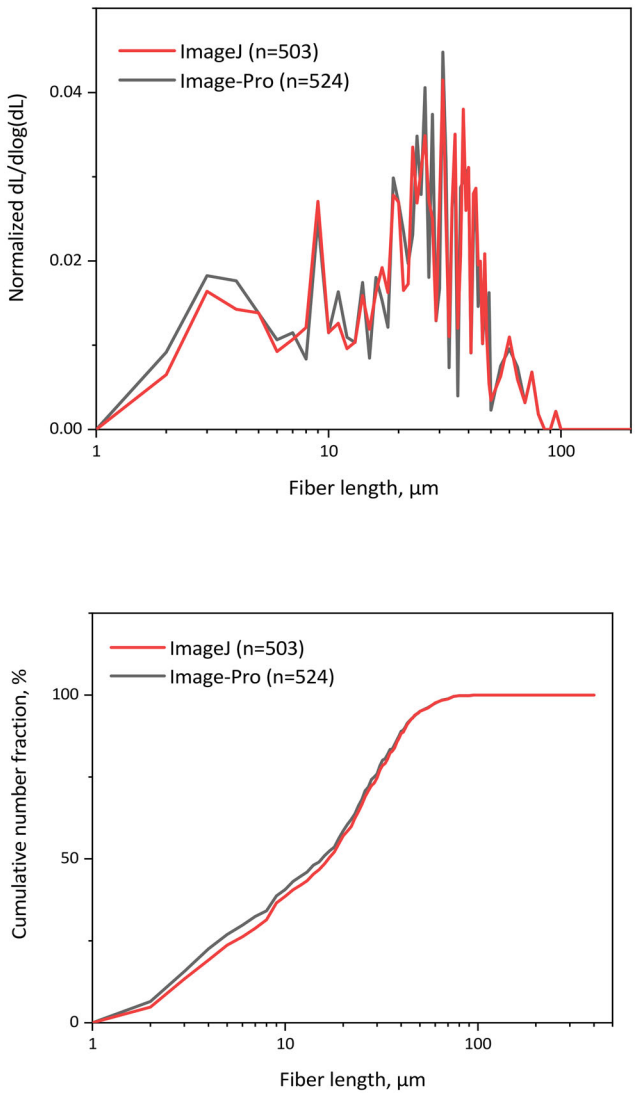

Figure 4. Normalized amosite length distributions and cumulative plots of ImageJ and Image-Pro measurement.

(PROC NPAR1WAY, SAS V 9.4) was conducted to compare length and width distributions between ImageJ and Image-Pro. Fiber length distributions were not significantly different ($p > 0.05$), while fiber width distributions were significantly different ($p < 0.05$).

PCM and PLM images

An example of PCM and PLM images that were processed with Image-Pro software is shown in Figure 6. The fibers in the PCM images were bright for relatively thicker fibers and dark for relatively thinner fibers. Image-Pro can select either bright or dark-colored fibers in its segmentation function. When the dark-colored fibers were selected, the bright-colored fibers (indicated with circles in Figure 6) were not isolated as a fiber and vice versa. Therefore, PCM images were not further evaluated due to this limitation. However, PLM images showed that both thin and thick fibers were dark-colored and most of the fibers were segmented from the background of the images. Several fibers that were too thin were not segmented in the PLM image analysis procedure (indicated with circles in Figure 6), and the length and width of those fibers were assessed by a manual Image-Pro measurement. Scatter plots of fibrous grunerite length and width in the five different PLM images measured with ImageJ and Image-Pro (n = 216) are shown in Figure 7. Results of linear regression analyses are summarized within the plot area. The measured length of the fibrous grunerite ranged from 1.4 to 60 µm and the measured width ranged from 0.4 to 4.7 µm with both software. The slopes of the regression lines for length and width were 1.02 and 0.84, respectively, and the intercepts were 0.06 and 0.02, respectively. For fiber length, the value of R^2, 0.99, was virtually equal to 1, indicating that ImageJ measurements could be

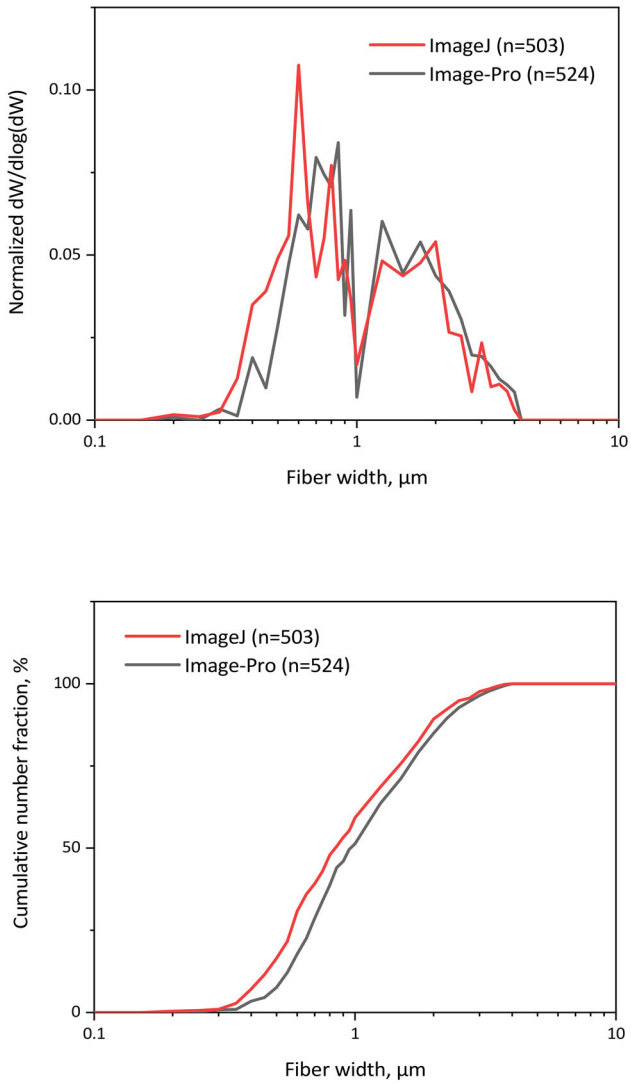

Figure 5. Normalized amosite width distributions and cumulative plots of ImageJ and Image-Pro measurement.

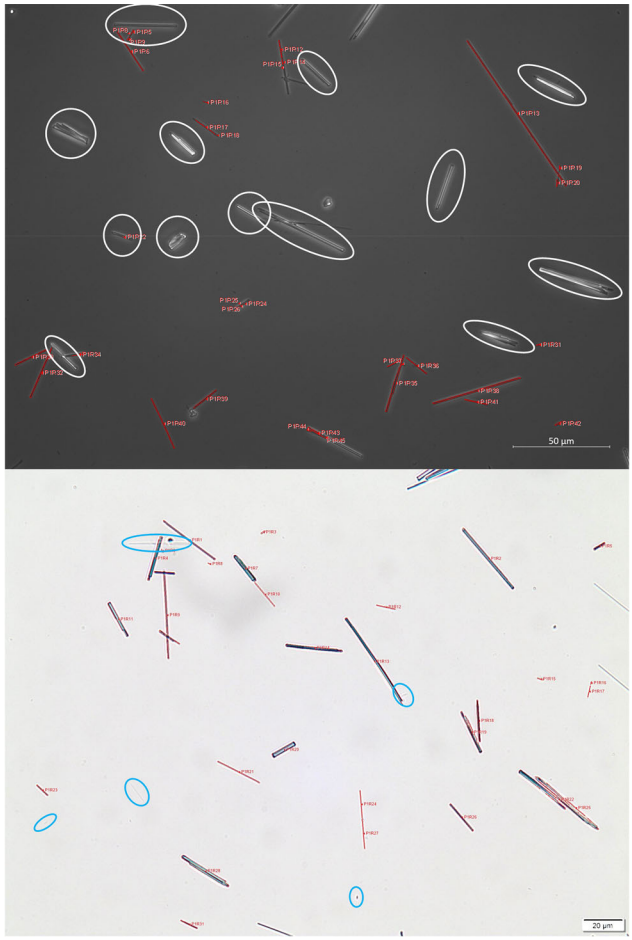

Figure 6. Examples of phase contrast microscope (top) and polarized light microscope (bottom) images processed with the Image-Pro software. White (top) and blue (bottom) circles indicate that the fiber was not recognized by the software.

predicted from Image-Pro measurements with negligible error. The value of R^2 for width, 0.92, was somewhat lower, indicating that approximately 92% of the variation in ImageJ measurements could be explained by Image-Pro measurements (Table 2). The relationship between length measurements of the two software with the PLM images was close to being perfect, while 8% of the variance in ImageJ width measurements was not explained by Image-Pro measurements. When measuring width in PLM images, it was difficult to define the edge of a fiber because resolution was lower than in SEM images and resulted in a significant difference between the measurements. The digital camera in the PLM has 3.1 mega pixels with 400× magnification. There were 6.3 pixels per micron and at least 2 pixels comprising the fiber width. A digital camera that had more mega pixels and smaller pixel size together with higher magnification (up to 1,000×) would be likely to make the edges of fibers in PLM images easier to define. Another possible reason for the difference between ImageJ and Image-Pro may be the difference in width measurements for fibers with a tapered or split end. When 16 pairs of width measurements reflecting large differences between the software were considered to be outliers and excluded from the regression analysis, the values of the slope and R^2 increased to 0.93 and 0.97, respectively. The normalized and cumulative fibrous grunerite length and width distributions in two different sets are shown in Figures 8 and 9, respectively. The data in these figures were first measured with Image-Pro in seven PLM images ($n = 217$), and second measured manually with ImageJ in seven PLM images ($n = 198$). The Kolmogorov–Smirnov tests found that fiber length distributions were not significantly different ($p > 0.05$), while fiber width distributions between the software were significantly different ($p < 0.05$). A consistent result was found between the linear regression analysis in the individual measurement comparison and the

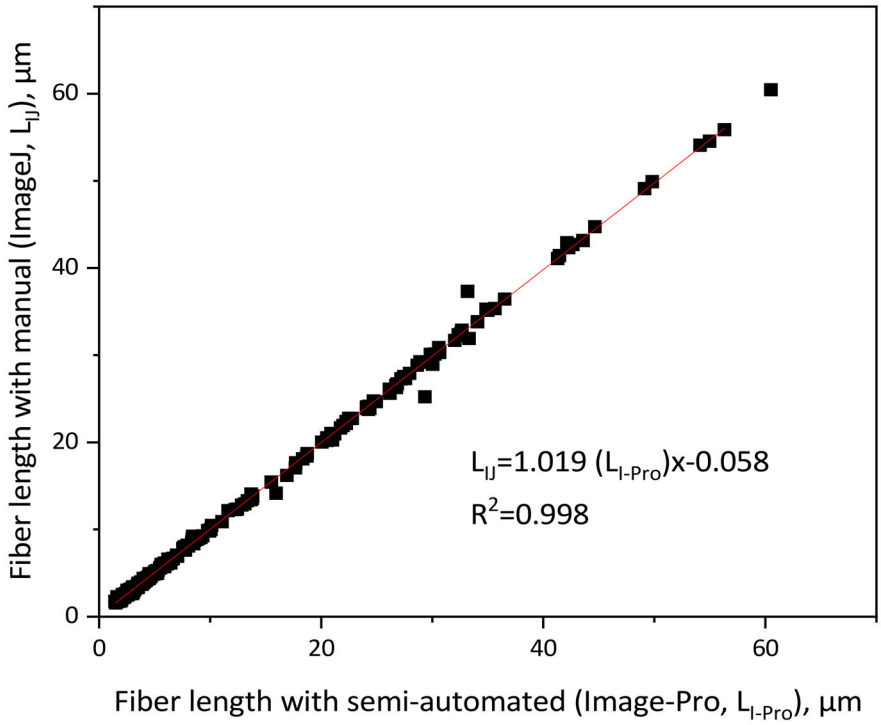

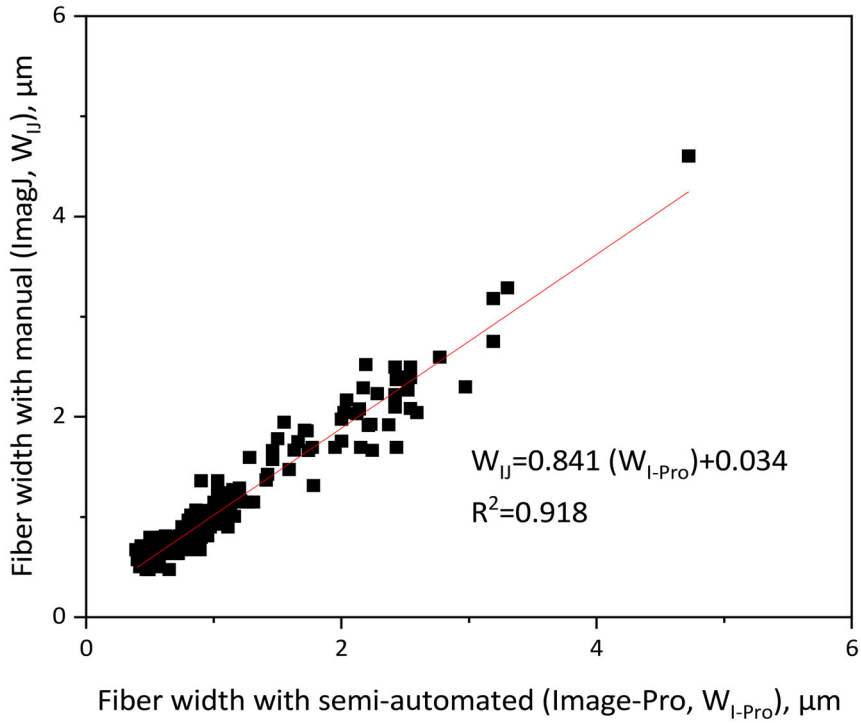

Figure 7. Scatter plot and linear regression analysis of amosite asbestos length and width measured with ImageJ and Image-Pro (n = 216, PLM images).

Kolmogorov–Smirnov test in length and width distribution comparison. If only the fiber length is of interest, the length measurement with PLM images was equally as good as with higher resolution SEM images.

One limitation of the current study is that attached or overlapped fibers were recognized as a single fiber in the procedure of the Image-Pro analysis, and manual intervention was needed to select the fibers that

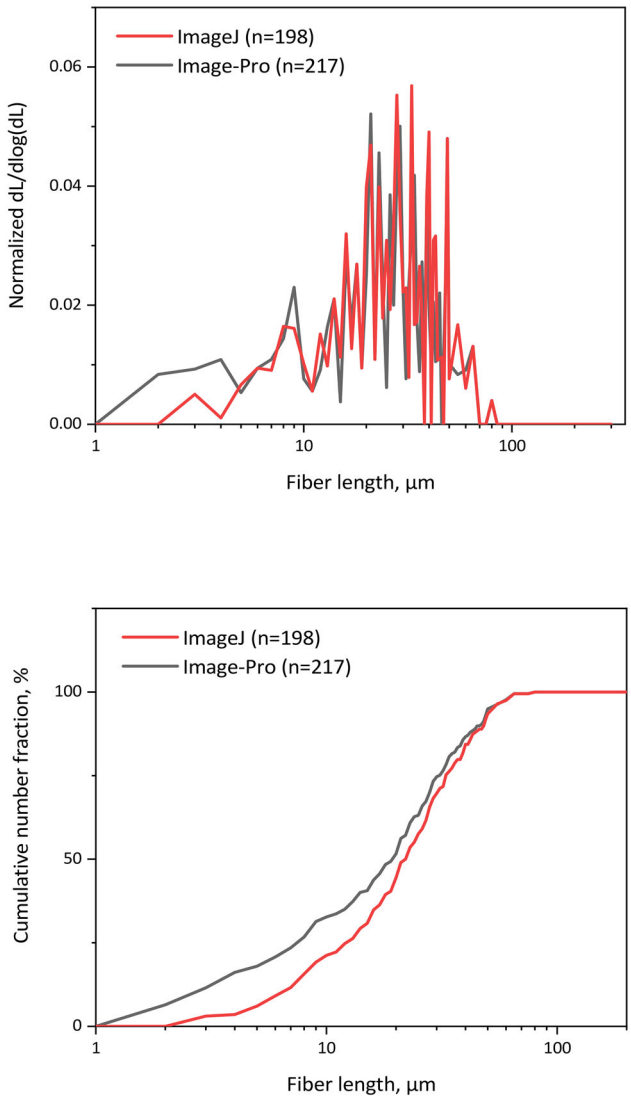

Figure 8. Normalized amosite length distributions and cumulative plots of ImageJ and Image-Pro measurement.

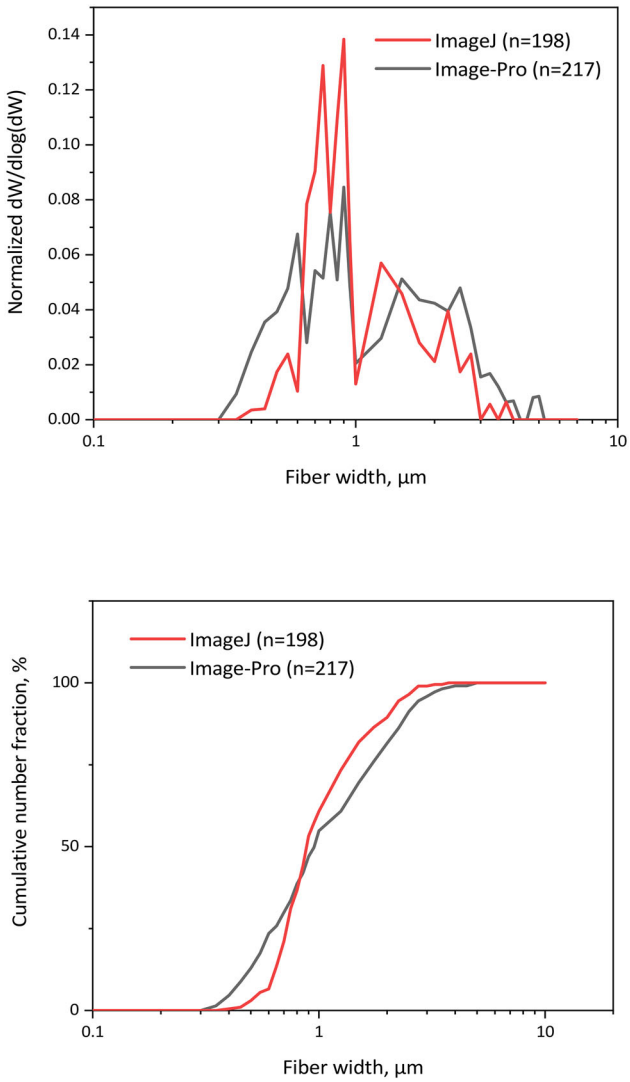

Figure 9. Normalized amosite width distributions and cumulative plots of ImageJ and Image-Pro measurement.

overlapped. The need for manual intervention may be overcome by optimizing sample preparation and employing an additional Image-Pro application. Samples should be carefully prepared through deagglomeration and dilution to reduce the incidence of attached or overlapped fibers. Utilization of a mixed solution of distilled water and dishwashing liquid may be helpful to disperse fibers in the samples (Siegrist and Wylie 1980). For the fibers that remain agglomerated, an additional Image-Pro application is needed. A fiber separation application for Image-Pro is offered as a free download by the original software developer (Media Cybernetics 2015) and will be evaluated in a future study.

Another limitation of the current study is that Image-Pro performance was not evaluated for curved fibers. Straight rather than curved fibers were used because the analysis involves a simpler process and would help with determining causes of method inaccuracies. If the software performed well for straight fibers, it would be reasonable to pursue the evaluation for curved fibers. The results showed that Image-Pro performed very well in measuring asbestos fiber length but not as well for width. Inaccuracies in the width measurement can be attributed to the modest PLM digital camera resolution and the appearance of bright fringes at the fiber perimeter. These effects tend to lead to an overestimation of width, which is implied by slopes less than one (Table 2) with Image-Pro measurements as the independent variable (on the x-axis). It is suggested to improve the resolution by using a 10 megapixel digital camera and by opening the aperture diaphragm to reduce bright fringes in PLM images. The presence of fibers with split or tapered ends can also lead to inaccuracies in the width measurement. The effect of irregular ends can be

studied using the Fiber Thickness application (Media Cybernetics 2019) for Image-Pro. This application allows the user to define the location(s) where the width is measured, such as at the fiber center (where the manual measurement was made) or at regular intervals along the main axis, and can be used to troubleshoot the discrepancy with ImageJ measurements. However, fiber length cannot be measured with the Fiber Thickness application, and it is therefore not a solution for the objective of the current study. The suggested adjustments and troubleshooting method for fiber width measurements will be tested in a future study, which will focus on PLM due to its lower cost and similar performance to SEM for lengths as small as 0.5 µm. This future study will also include an evaluation of Image-Pro performance using TEM images as a best case for image resolution. Although the width measurement can be improved, the current evaluation showed that Image-Pro provided a reasonable estimate. The R^2 value for width indicated that approximately 92% and 97% of the variation in ImageJ measurements could be explained by Image-Pro measurements in PLM and SEM images, respectively (Table 2). Consequently, Image-Pro can be used for concurrent measurements of length and width, under the assumption that the width measurement is an approximate value.

If the width measurement is improved, the performance of Image-Pro will be evaluated for curved asbestos fibers, fiber bundles, and subsequently for a mix of particles representative of environmental samples, including soot, dust, and asbestos fibers. If the fibers are efficiently detected in mixed samples, the automated measurement may become a candidate for a new standard method of asbestos and other fiber analysis. It would be similar to standard methods that utilize PCM, which only require measuring up to 100 fibers due to excessive manual analysis times (Baron 2016), but would have the advantage that lower concentrations could be measured because thousands of particles could be analyzed in a fraction of the time. PLM rather than PCM images would be used because PCM images are not suitable for automated analysis due to a lack of consistent contrast with the background. Specifically, some fibers (usually thin) were darker than the background, others (usually thick) were brighter than the background, and some individual fibers had sections that were both brighter and darker than the background (Figure 6, top). For samples that contain mostly fibers, the automated method can be used measure a statistically significant number of particles and obtain a representative size distribution for the length, width, and calculated aerodynamic diameter.

Fritzsch et al. (2013) reported that the time required to measure 32,509 particles in 700 light microscope images manually and using Image-Pro Plus (Version 7.0) was 6 months and 1 hr, respectively. The analysis time with Image-Pro per image in the present study was less than a minute when excluding time for the corrections due to attaching or overlapping fibers. For manual measurements, the analysis time was dependent on the number of fibers in an image, although it generally ranged from 30 min to 60 min per image.

Conclusions

Manual and semi-automated image analysis methods for asbestos fibers were compared using PCM, PLM, and SEM images to determine if a fast method for concurrent measurements of fiber length and width could be obtained with Image-Pro software. It was found that PCM images were not suitable for semi-automated analysis because there was a lack of consistent contrast with the background. Some individual fibers appeared brighter than the background, others were darker, and a few individual fibers had brighter and darker sections. However, asbestos fibers in PLM and SEM images had consistent contrast and could be characterized by semi-automated analysis. Based on the results of the present study, length measurements in PLM and SEM images with ImageJ and Image-Pro software showed a nearly 1:1 relationship. Measurements using PLM images were as accurate as those for SEM for fibers lengths as short as 0.5 µm. The width measurements of ImageJ and Image-Pro did not show as strong of a relationship for either PLM or SEM images. However, reasonable estimates for width were obtained, in that, 92% and 97% of the variance in ImageJ measurements could be explained by Image-Pro using PLM and SEM images, respectively. Because of attached and overlapping fibers, the analysis with Image-Pro was not a fully automated procedure. Yet, it is still a fast and reasonably accurate procedure when compared to time-consuming manual measurements of fiber length and width.

Disclaimer

The findings and conclusions in this report are those of the authors and do not necessarily represent the official position of the National Institute for Occupational Safety and Health, Centers for Disease Control and Prevention. Mention of any company or product does not constitute endorsement by NIOSH.

Funding

National Institute for Occupational Safety and Health, Project #9390BMJ: Understanding elongate mineral particle exposure in mining.

References

Baron PA. 2016. Measurement of fibers, manual of analytical methods. 5th ed. Cincinnati (OH): National Institute for Occupational Safety and Health. p. FI1–FI31.

Baumann F, Ambrosi JP, Carbone M. 2013. Asbestos is not just asbestos: an unrecognised health hazard. Lancet Oncol. 14(7):576–578. doi:10.1016/S1470-2045(13)70257-2

Blake T, Castranova V, Schwegler-Berry D, Deye GJ, Baron P, Li C, Jones W. 1997. Effect of fiber length on glass microfiber cytotoxicity. J Tox Environ Health. 54A:243–259.

Cossio R, Albonico C, Zanella A, Fraterrigo-Garofalo S, Avataneo C, Compagnoni R, Turci F. 2018. Innovative unattended SEM-EDS analysis for asbestos fiber quantification. Talanta. 190:158–166. doi:10.1016/j.talanta.2018.07.083

Fritzsch R, Mirzaei B, Kennedy MW, Aune RE. 2013. Automated quantification of SiC-particles in solidified A356 aluminium using Image-Pro plus 7.0. The Minerals Metals and Materials Society Annual Meeting; March 3–7, 2013; San Antonio, Texas, USA, p. 69–77.

Fujimoto Y, Urashima T, Shimura D, Ito R, Kawachi S, Kajimura I, Akaike T, Kusakari Y, Fujiwara M, Ogawa K, et al. 2016. Low cardiac output leads hepatic fibrosis in right heart failure model rats. PLoS One. 11(2):e0148666. doi:10.1371/journal.pone.0148666

Goris S, Back T, Yanev A, Brands D, Drummer D, Osswald TA. 2018. A novel fiber length measurement technique for discontinuous fiber-reinforced composites: a comparative study with existing methods. Polym Compos. 39(11):4058–4070. doi:10.1002/pc.24466

Götz A, Senz V, Schmidt W, Huling J, Grabow N, Illner S. 2021. General image fiber tool: a concept for automated evaluation of fiber diameters in SEM images. Measurement. 177:109265. doi:10.1016/j.measurement.2021.109265

Harper M, Van Gosen B, Crankshaw OS, Doorn SS, Ennis TJ, Harrison SE. 2015. Characterization of Lone Pine, California, tremolite asbestos and preparation of research material. Ann Occup Hyg. 59(1):91–103. doi:10.1093/annhyg/meu074

Hartwich MR, Höhn N, Mayr H, Sandau K, Stengle R. 2009. FASEP ultra-automated analysis of fibre length distribution in glass-fibre-reinforced products. Proceedings of SPIE 7389, Optical Measurement Systems for Industrial Inspection VI, Munich, Germany, 738921. doi:10.1117/12.827503

Hotaling NA, Bharti K, Kriel H, Simon CG. 2015. DiameterJ: a validated open source nanofiber diameter measurement tool. Biomaterials. 61:327–338. doi:10.1016/j.biomaterials.2015.05.015

Lee T, Ku BK, Walker R, Kulkarni P, Barone T, Mischler S. 2020. Aerodynamic size separation of glass fiber aerosols. J Occup Environ Hyg. 17(6):301–311. doi:10.1080/15459624.2020.1742915

Lee T, Walker R, Hummer J, Ashley E, Mischler S. 2021. Size separation of amosite by filtration and shaking methods. In Millette JR, Webber JS, editors Asbestos and other elongate mineral particles—new and continuing challenges in the 21st century. West Conshohocken (PA): ASTM International. p. 265–280. doi:10.1520/STP163220200067.

Lippmann M. 1988. Asbestos exposure indices. Environ Res. 46(1):86–106. doi:10.1016/s0013-9351(88)80061-6

Liu C, Bergmeijer M, Pierrat S, Guise O. 2020. Automatic fiber length measurements with a multi-stencil fast marching method on microscopy images. Microsc Microanal. 26(3):387–396. doi:10.1017/S1431927620001336

Media Cybernetics. 2015. Fiber separation; [accessed 2021 Dec 28]. https://www.mediacy.com/support/imageproinsight/appcenter/fiber-separation-application-detail.

Media Cybernetics. 2019. Fiber thickness; [accessed 2021 Dec 28]. https://www.mediacy.com/support/imageproinsight/appcenter/fiber-thickness-detail.

Ma X, Cogswell A, Li Z, Lee K. 2008. Particle size analysis of dispersed oil and oil-mineral aggregates with an automated ultraviolet epi-fluorescence microscopy system. Environ Technol. 29(7):739–748. doi:10.1080/09593330801987111

Murphy R, Turcott A, Banuelos L, Dowey E, Goodwin B, Cardinal KOH. 2020. SIMPoly: a Matlab-based image analysis tool to measure electrospun polymer scaffold fiber diameter. Tissue Eng Part C Methods. 26(12):628–636. doi:10.1089/ten.TEC.2020.0304

National Institute for Occupational Safety and Health. 1979. Preparation and characterization of analytical reference minerals. Department of Health, Education, and Welfare. Cincinnati (OH): National Institute for Occupational Safety and Health, Publication No. 79–139.

Primpke S, Dias PA, Gerdts G. 2019. Automated identification and quantification of microfibres and microplastics. Anal Methods. 11(16):2138–2147. doi:10.1039/C9AY00126C

Reedy C, Anderson J, Reedy T. 2017. Quantitative porosity studies of archaeological ceramics by petrographic image analysis. MRS Proc. 1656:337–353. doi:10.1557/opl.2014.711

Schneider CA, Rasband WS, Eliceiri KW. 2012. NIH Image to ImageJ: 25 years of image analysis. Nat Methods. 9(7):671–675. doi:10.1038/nmeth.2089

Siegrist HG, Wylie AG. 1980. Characterizing and discriminating the shape of asbestos particles. Environ Res. 23(2):348–361. doi:10.1016/0013-9351(80)90070-5

Skinner HCW, Ross M, Frondel C. 1988. Asbestos and other fibrous materials: mineralogy, crystal chemistry and health effects. New York (NY): Oxford University Press. p. 94.

Stevens CR, Berenson J, Sledziona M, Moore TP, Dong L, Cheetham J. 2020. Approach for semi-automated measurement of fiber diameter in murine and canine skeletal muscle. PLoS One. 15(12):e0243163. doi:10.1371/journal.pone.0243163

Wang W, Itoh S, Matsuda A, Ichinose S, Shinomiya K, Hata Y, Tanaka J. 2008. Influences of mechanical properties and permeability on chitosan nano/microfiber mesh tubes as a scaffold for nerve regeneration. J Biomed Mater Res A. 84(2):557–566. doi:10.1002/jbm.a.31536

Xu B, Ting YL. 1996. Fiber-image analysis part II: measurement of general geometric properties of fibers. J Text Inst. 87(2):284–295. doi:10.1080/00405009608659081

Zhang XM, Wang RW, Wu HB, Xu B. 2014. Automated measurements of fiber diameters in melt-blown nonwovens. J Ind Text. 43(4):593–605. doi:10.1177/1528083712471696